ARL-TR-8877 ● Dec 2019

DEVCOM ARMY RESEARCH LABORATORY

# Constrained Geometry Relative Swarm Localization

by Mitchell J Grabner, Michael L Don, and Daniel P Everson

## NOTICES

### Disclaimers

The findings in this report are not to be construed as an official Department of the Army position unless so designated by other authorized documents.

Citation of manufacturer's or trade names does not constitute an official endorsement or approval of the use thereof.

Destroy this report when it is no longer needed. Do not return it to the originator.

ARL-TR-8877 ● DEC 2019


# Constrained Geometry Relative Swarm Localization

**Mitchell J Grabner**
*University of North Texas*

**Michael L Don and Daniel P Everson**
*Weapons and Materials Research Directorate, CCDC Army Research Laboratory*

# REPORT DOCUMENTATION PAGE

*Form Approved*
*OMB No. 0704-0188*



| 1. REPORT DATE *(DD-MM-YYYY)* | 2. REPORT TYPE | 3. DATES COVERED (From - To) |
|---|---|---|
| December 2019 | Technical Report | 1–30 August 2018 |

**4. TITLE AND SUBTITLE**
Constrained Geometry Relative Swarm Localization

**5a. CONTRACT NUMBER**

**5b. GRANT NUMBER**

**5c. PROGRAM ELEMENT NUMBER**

**6. AUTHOR(S)**
Mitchell J Grabner, Michael L Don, and Daniel P Everson

**5d. PROJECT NUMBER**

**5e. TASK NUMBER**

**5f. WORK UNIT NUMBER**

**7. PERFORMING ORGANIZATION NAME(S) AND ADDRESS(ES)**
CCDC Army Research Laboratory*
ATTN: FCDD-RLW-LF
Aberdeen Proving Ground, MD 21005-5066

**8. PERFORMING ORGANIZATION REPORT NUMBER**
ARL-TR-8877

**9. SPONSORING/MONITORING AGENCY NAME(S) AND ADDRESS(ES)**

**10. SPONSOR/MONITOR'S ACRONYM(S)**

**11. SPONSOR/MONITOR'S REPORT NUMBER(S)**

**12. DISTRIBUTION/AVAILABILITY STATEMENT**
Approved for public release; distribution is unlimited.

**13. SUPPLEMENTARY NOTES**
* The work outlined in this report was performed while the US Army Research Laboratory (ARL) was part of the US Army Research, Development, and Engineering Command (RDECOM). As of 31 January 2019, the organization is now part of the US Army Combat Capabilities Development Command (formerly RDECOM) and is now called CCDC Army Research Laboratory.

**14. ABSTRACT**
Operating in GPS-denied environments presents many challenges when accurate positioning, navigation, and timing information is required. A simple way of alleviating many of these problems without complex infrastructure is by employing swarms of cooperative agents instead of utilizing solitary individuals. In real-use cases like unmanned aerial vehicle missions or munition delivery, optimum swarm geometries cannot be used because the location of other agents, other equipment, or even terrain obstruct correct positioning. In this report, we develop a high-performance constrained swarm geometry and characterize it based on its Z-dimension standard deviation, position root mean square error, and dilution of precision. We further characterize the Nanotron SwarmBee ranging device's long-range accuracy and performance in a multipath environment. Lastly, we conduct a real-world test of our best constrained geometry and compare its performance to our simulated results.

**15. SUBJECT TERMS**
RF ranging, DOP, swarm localization, swarm geometry, swarm networking, Nanotron

| 16. SECURITY CLASSIFICATION OF: | | | 17. LIMITATION OF ABSTRACT | 18. NUMBER OF PAGES | 19a. NAME OF RESPONSIBLE PERSON |
|---|---|---|---|---|---|
| a. REPORT | b. ABSTRACT | c. THIS PAGE | | | Michael L Don |
| Unclassified | Unclassified | Unclassified | UU | 51 | 19b. TELEPHONE NUMBER (Include area code) 410-306-0775 |

## Contents

## List of Figures

## List of Tables

# 1. Introduction

Operating in GPS–denied environments presents many challenges when accurate positioning, navigation, and timing information is required.[1] One method of alleviating many of these problems without complex infrastructure is by employing swarms of cooperative agents instead of singular assets. The main advantage of this approach is the ability for swarm agents to localize relative to the group, using distance and other spatial relationships to achieve accurate relative position information and therefore reduce reliance on external sensory information such as GPS.[2] Swarm relative localization has many applications such as location-aware networking protocols,[3] collision avoidance,[4] formation flying[5] and patterned weapon delivery.[6]

One method to achieve relative swarm localization is through estimating agent positions from noisy range measurements between agents. A key performance metric in such a localization scheme is the agents' estimated position accuracy. This accuracy is not solely based on the quality of the range measurements, as swarm geometry plays an important role in localization error.[7] The relationship between the agent's geometry and localization error is called dilution of precision (DOP), and is commonly used in GPS error characterization.[8] Just as the GPS satellite constellations were carefully constructed to limit the amount of DOP experienced by GPS receivers, so too swarm geometry must be designed to minimize the DOP of the swarm agents.

Although the GPS DOP metric is a good starting point for consideration of a swarm DOP metric, GPS DOP cannot be directly applied to relative swarm localization for three reasons. First, GPS uses one-way time-of-flight (TOF) ranging, which requires synchronization and the receiver's clock bias to be factored into the DOP measurements. Typical swarm range measurements use two-way ranging (TWR), which is independent of clock bias and syncronization.[9] Second, GPS satellites have known absolute positions that are used to determine the receiver's location. Thus, a single DOP value characterizes the quality of satellites' geometry with respect to the receiver. In swarm relative localization all of the agents' positions are unknown and their locations must be solved collectively, forcing us to consider the geometry of the swarm with respect to each agent. Third, since the absolute positions of the satellites are known, the absolute position of the receiver can also be found. This makes it straightforward to measure receiver's position error. In contrast, relative swarm localization lacks absolute position information, therefore requiring alignment to reference positions in order to evaluate solution accuracy and precision.

In this report, we will briefly review the DOP metric for localization using TWR[1] and the swarm relative localization method using the classical multidimensional scaling (MDS)[10] and Kabsch[11] algorithms. We will conclude the review with optimum relative localization swarm geometries for different number of agents and characterize their DOP and the root mean square error (RMSE).[1] Expanding on the previous work we will look at constrained geometries with only five stationary agents where the availability of agent locations in the Z-dimension is limited to 2.5 m. We explore four different swarm geometry designs and characterize them based on agents' error from their reference positions and also their deviation in the Z-dimension. We then compare the DOP of all four designs and discuss the relationship between their DOP and RMSE.

The experimental design sections of the report start with a survey of various antennas implemented on the same Nanotron SwarmBee TWR devices used in previous work.[12] A reliability study is presented that selects the highest performing antenna that minimizes the number of dropped measurements. Next, we look at the performance of all six of our SwarmBee test units to verify consistent operation in a multipath environment. We then conduct a long-range test to characterize maximum distance performance in a controlled, low-multipath and noise-free environment. The final experiment we conduct is a real-world test of our best constrained geometry in a benign environment. We compare the results of this experiment to our simulated data and modify the simulation environment to better match our experimental results. Lastly, we conclude with our overall thoughts and further research goals.

## 2. Summary of TWR, Swarm Relative Localization, and DOP

Position tracking systems such as GPS use TOF ranging that requires expensive infrastructure to synchronize the clocks on the GPS satellites. This one-way TOF ranging is ideal for GPS due to the large distances between the agent and the satellites. In the case of smaller geometries, like those typically used for relative swarm localization, TWR can be used to range between agents. This method is independent of time synchronization, which reduces system requirements. A typical single-sided TWR range measurement $p$ in meters between two agents $a$ and $b$ can be written as

$$p = \frac{c(t_{ab}+t_{ba})}{2} + e, \tag{1}$$

where $c$ is the speed of light in meters per second, $t_{ab}$ and $t_{ba}$ are the travel times in fractions of a second from agent $a$ to agent $b$ and agent $b$ to agent $a$, respectively, and $e$ is the error due to noise. In the case of a swarm of $n$ agents, none of the agent

positions are known, requiring an algorithm to solve for the relative localization of the agents. One such algorithm is classical MDS,[13] which proceeds as follows. Let $\boldsymbol{D}^{\odot 2} \in \mathbb{R}^{n\times n}$ be the squared Euclidean range measurement matrix composed of elements $p_{ij}^2$ representing the squared range measurement from agent $i$ to agent $j \neq i, 1 \leq i, j \leq n$. The Hadamard (element-wise) exponentiation is denoted as $(\,.\,)^{\odot 2}$. $\boldsymbol{D}^{\odot 2}$ is double centered by

$$\boldsymbol{B} = -\frac{1}{2}\boldsymbol{C}\boldsymbol{D}^{\odot 2}\boldsymbol{C}, \tag{2}$$

where $\boldsymbol{C}$ is the centering matrix

$$\boldsymbol{C} = \boldsymbol{I} - \frac{1}{n}\mathbb{O}. \tag{3}$$

$\boldsymbol{I} \in \mathbb{R}^{n\times n}$ is the identity matrix, and $\mathbb{O} \in \mathbb{R}^{n\times n}$ is a matrix of all 1s. The agent location matrix $\boldsymbol{X} \in \mathbb{R}^{n\times 3}$ is then the first three columns of $\boldsymbol{X}'$ given by

$$\boldsymbol{X}' = \boldsymbol{E}\boldsymbol{\Lambda}^{\odot 1/2} \tag{4}$$

where $\boldsymbol{E}$ is a matrix of the $n$ eigenvectors of $\boldsymbol{B}$, and $\boldsymbol{\Lambda}$ is a diagonal matrix of the corresponding $n$ eigenvalues of $\boldsymbol{B}$ in descending order.

Since only the relative localization is determined, localization calculations may differ in rotation, translation, and reflection from reference positions defined in an absolute coordinate frame. This makes it difficult to calculate localization error relative to the reference frame in simulation, as an alignment must be performed. In order to align swarm positions they can be rotated, translated, and reflected to minimize the RMSE to given reference points using the Kabsch algorithm.[11] For swarm localization simulations, the true stationary agent positions $\boldsymbol{X}_1$ are used as reference for the estimated location matrix $\boldsymbol{X}_2$. The Kabsch algorithm starts by calculating and subtracting the centroids of $\boldsymbol{X}_1$ and $\boldsymbol{X}_2$ giving

$$\boldsymbol{P}_1 = \boldsymbol{X}_1 - \frac{1}{n}\mathbb{O}\boldsymbol{X}_1 \tag{5}$$

and

$$\boldsymbol{P}_2 = \boldsymbol{X}_2 - \frac{1}{n}\mathbb{O}\boldsymbol{X}_2. \tag{6}$$

Next, the cross covariance matrix is calculated as

$$\boldsymbol{A} = \frac{1}{n}\boldsymbol{P}_1^T\boldsymbol{P}_2. \tag{7}$$

Using singular value decomposition, $\boldsymbol{A}$ is represented as

$$\boldsymbol{A} = \boldsymbol{U}\boldsymbol{W}\boldsymbol{V}^T. \tag{8}$$

The rotation matrix is then

$$\boldsymbol{R} = \boldsymbol{U}\boldsymbol{V}^T \tag{9}$$

and the translation is

$$\boldsymbol{t} = \frac{1}{n}\boldsymbol{X}_1^T\boldsymbol{1} - \frac{1}{n}\boldsymbol{X}_2^T\boldsymbol{1}\boldsymbol{R}, \tag{10}$$

where $\boldsymbol{1} \in \mathbb{R}^{n\times 1}$ is a vector of all 1s. Typical applications of the Kabsch algorithm ensure $|\boldsymbol{R}| \geq 0$ to prevent reflection. Here reflection is allowed to correct for any reflection caused by the classical MDS algorithm.

DOP measures the degree to which range measurement errors affect the accuracy of the agent's position. The DOP of an agent at position $\boldsymbol{x} \in \mathbb{R}^3$ is calculated with respect to $m = n - 1$ other agents with positions $\boldsymbol{a}_s \in \mathbb{R}^3$ for $1 \leq s \leq m$. Using the Jacobian matrix $\boldsymbol{J} \in \mathbb{R}^{m\times 3}$ defined as

$$J_{sk} = \frac{x_k - a_{sk}}{\|\boldsymbol{x} - \boldsymbol{a}_s\|}, \tag{11}$$

where $1 \leq k \leq 3$, the matrix $\boldsymbol{Q} \in \mathbb{R}^{3\times 3}$ is formulated as

$$\boldsymbol{Q} = (\boldsymbol{J}^T\boldsymbol{J})^{-1}. \tag{12}$$

The diagonal elements of $\boldsymbol{Q}$ are the variances of $x_k$

$$Q_{kk} = \sigma_{x_k}^2. \tag{13}$$

For TWR localization, DOP values are expressed as[7]

- X-dimension DOP (XDOP)
- Y-dimension DOP (YDOP)
- Z-dimension DOP (ZDOP)
- Position DOP (PDOP)

Using $x$, $y$, and $z$ for the elements of $\boldsymbol{x}$, these DOP values are

$$XDOP = \sqrt{\sigma_x^2}, \tag{14}$$

$$YDOP = \sqrt{\sigma_y^2}, \tag{15}$$

$$ZDOP = \sqrt{\sigma_z^2}, \tag{16}$$

$$PDOP = \sqrt{\sigma_x^2 + \sigma_y^2 + \sigma_z^2}. \tag{17}$$

An intuitive example of DOP can be seen in Fig. 1. Three stationary agents are shown as orange circles and the agent we wish to find the position of is shown as a small black circle. A range measurement from agent to the agent, denoted as $p$, limits the possible positions of the agent in two dimensions to a circle around the anchor with radius $p$. With the addition of measurement noise, this circle transforms into a region where the red circles designate an upper bound on the true range and the green circles designate a lower bound. The area where these regions overlap is colored blue, and bounds the possible location of the agent. In the example on the left the three anchors are spread out around the agent, creating a small region of uncertainty for the agent, indicating a small DOP. On the right, the anchors are close together, resulting in a larger region of uncertainty indicating a large DOP.[1]

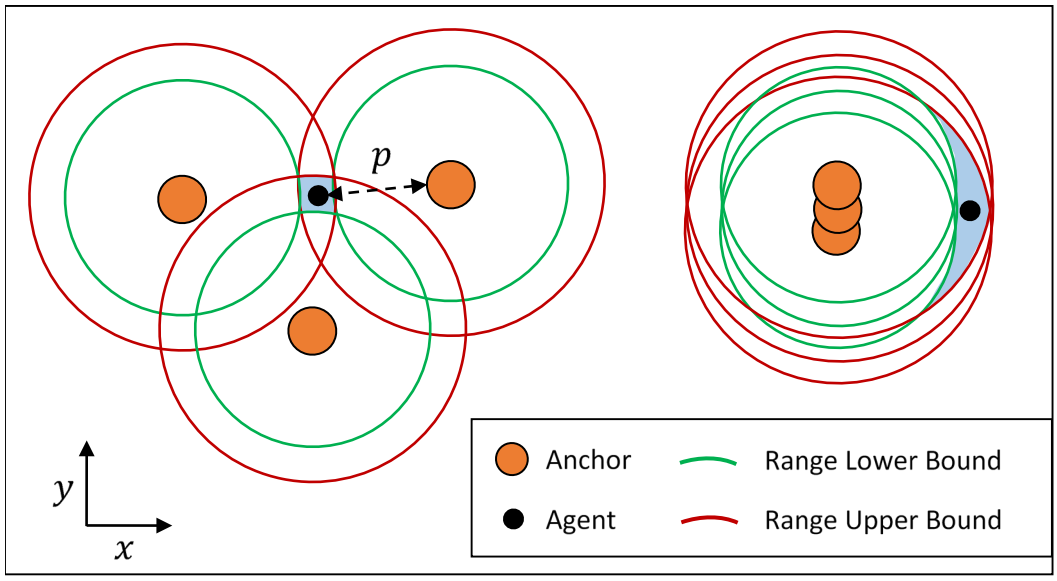


**Fig. 1 Example of a simple 2-D geometry with low DOP (left) and high DOP (right)[1]**

# 3. Constrained vs. Optimum Swarm Geometries

## 3.1 Optimum Geometries

In the previous work,[1] four platonic solids were chosen that should have optimal DOP values due to their symmetric geometry.[8] Intuitively, the greater the number of swarm agents, the lower the DOP, and the lower the resulting position RMSE. 100 simulations were run for each case with unbiased Gaussian noise with standard deviation $\sigma = 0.5$ added to the range measurements. Table 1 summarizes the results, listing the average TWR PDOP according to Eq. 15 and RMSE for all of the agents according to

$$e_{rmse} = \sqrt[2]{\frac{1}{n}\sum_{i=1}^{n}(\boldsymbol{x}_i - \boldsymbol{r}_i)^2} \tag{18}$$

where $\boldsymbol{x}_i$ and $\boldsymbol{r}_i$ are the estimated agent and known reference positions for each of the $n$ agents in $\mathbb{R}^3$, respectively. The estimated agent positions for the four cases are also shown in Fig. 2. As expected, the RMSE decreases with the PDOP.

**Table 1 PDOP and RMSE values for different optimum geometries**

| Swarm geometry | $n$ agents | PDOP | RMSE |
|---|---|---|---|
| Octahedron | 6 | 1.53 | 0.42 |
| Cube | 8 | 1.26 | 0.38 |
| Icosahedron | 12 | 0.98 | 0.34 |
| Dodecahedron | 20 | 0.74 | 0.28 |

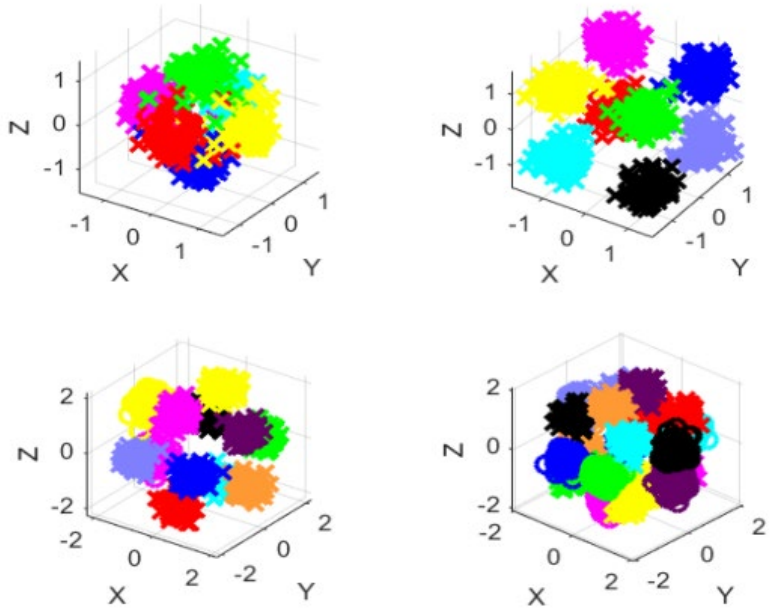


**Fig. 2 Four cases of swarm relative localization optimum geometries for different swarm sizes. The upper left has 6 agents, the upper right 8, lower left 12, and the lower right 20 agents.[1]**

## 3.2 Constrained Geometry Simulations

From the previous section we can see that as the number of swarm agents increases the optimum geometry starts to approximate a sphere around the origin. In real-use cases like GPS satellites, unmanned aerial vehicle missions, or munition delivery, optimum geometries cannot be used because the location of other agents, other equipment, or even terrain, obstruct correct positioning around a platonic solid. Therefore, it is useful to characterize geometry design under tight positioning and agent constraints to accurately evaluate relative swarm localization performance in a real scenario.

The constraints on our simulations are based on hardware and terrain limitations for ground-based experimental design. Our hardware is limited to six SwarmBee agents with tripods and ladders up to 2.5 m tall and an open, low multipath space of approximately $100 \times 100$ m. We define "low multipath" in the sense that there are no buildings or large vegetation in the test space. We also want to maximize TWR distance to stress the performance of our SwarmBee devices.

Using our understanding of the previous work on DOP and swarm relative localization as well as their optimum geometries, we developed a simple heuristic approach to constrained swarm design.

- Maintain symmetry whenever possible in order to maintain consistent DOP and position error[1,8]
- Place stationary agents on spheres whenever possible to reduce absolute DOP and position error[1,8]

For all subsequent simulations we use unbiased Gaussian noise with variance $\sigma^2 = 0.1$ added directly to the range measurements to simulate range estimation error. Since we also want to maximize our XY distance in order to stress our SwarmBee TWR performance, we opted for the maximum 50-m radius sphere in all our geometries. Our simulation analysis will evaluate four designs that conform to the constraints and heuristic design approach described previously.

Design 1 consists of five stationary agents equally spaced on the equator of a sphere centered at (0,0,1) and a mobile agent inside the stationary geometry orbiting in a 25-m radius circle with a Z-dimension height of 2 m.

Figures 3 and 4 depict the performance of Design 1 viewed from the XZ- and XY-planes, respectively. True stationary and mobile positions are denoted by red dots while the simulated position estimates using MDS and Kabsch are colored crosses for the stationary agents and a blue line for the mobile trajectory. For this and all subsequent swarm simulations in this research, agent 1 is the mobile, agent 2 is light blue, agent 3 is orange, agent 4 is yellow, agent 5 is purple, and agent 6 is green.

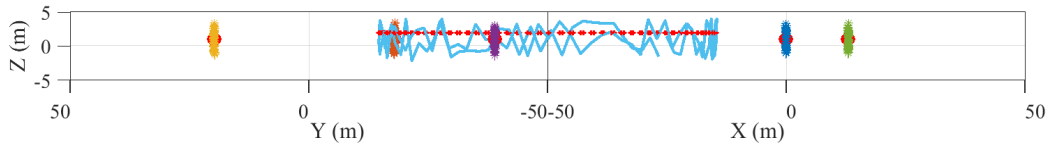


**Fig. 3 First swarm geometry XZ-plane with a 45° perspective with true locations (red) and estimated locations**

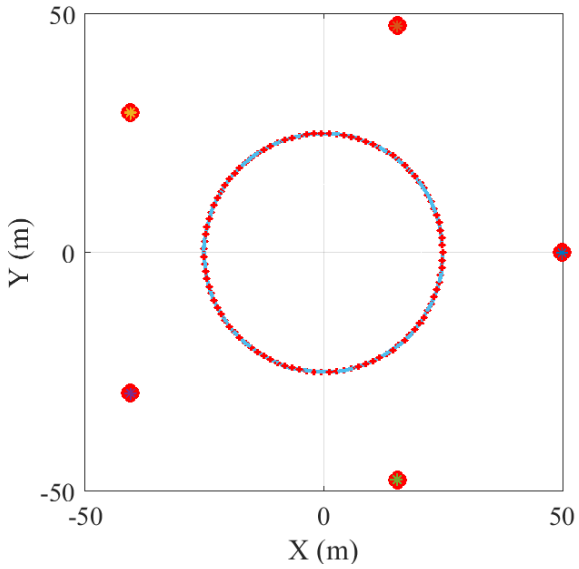


**Fig. 4 First swarm geometry XY-plane with true locations (red) and estimated locations**

As expected from a constrained geometry in the Z-dimension, we can see again in Fig. 3 that there is much variation in the Z-position estimates of both the stationary agents and the mobile agent. However, since our stationary locations in the XY-dimension are equally spaced around a sphere, Fig. 4 shows that there is negligible variation in the X- or Y-dimensions for all six agents. Figure 5 shows (left) the standard deviation of position estimates for all six agents in the Z-dimension and the position error in meters (right). For this and all subsequent box plots in this research, the central horizontal line indicates the median and the bottom and top of the box indicate the 25th and 75th percentiles, respectively. The dashed lines on either side of the box extend to the most extreme data points not considered outliers. Outliers are plotted individually as blue circles. We can see that all of the stationary agents have a consistent error and standard deviation thanks to the symmetrical geometry and fixed location. The mobile agent is inconsistent as its position relative to the stationary agents changes over time as it travels around the circle. Interestingly, since all the stationary agents are on the same XY-plane, the MDS method is not able to discern the Z-dimension of the mobile agent and estimates it to be in-plane with them. This is easily understood from the –1 median error in mobile agent 1 box plot.

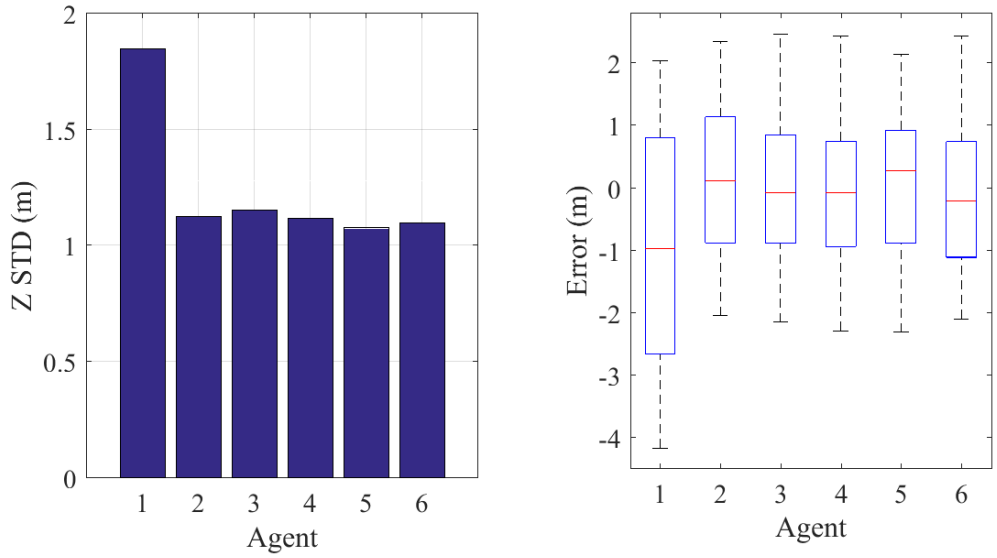


**Fig. 5 Standard deviation in Z (left) and position error (right) for the first swarm geometry in Figs. 3 and 4**

Since our first geometry simulation estimated all of the mobile positions on the same XY-plane as the anchor nodes, it is clear that diversity in the Z-dimension is required to accurately discern positions in $\mathbb{R}^3$ using the MDS method. Therefore, in Design 2, we move agents 2 and 4 up to 2.5 m in the Z-dimension while leaving stationary agents 3, 5, and 6 at a height of 1 m. Simulated performance of this geometry in the XZ- and XY-planes can be seen in Figs. 6 and 7, respectively.

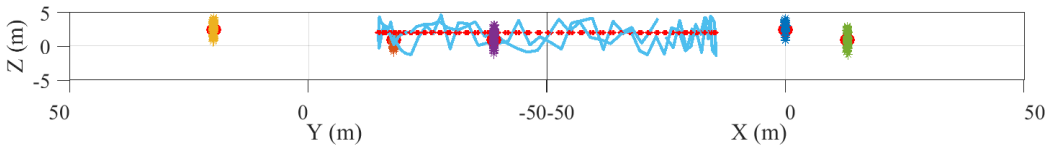


**Fig. 6 Second swarm geometry XZ-plane with a 45° perspective with true locations (red) and estimated locations**

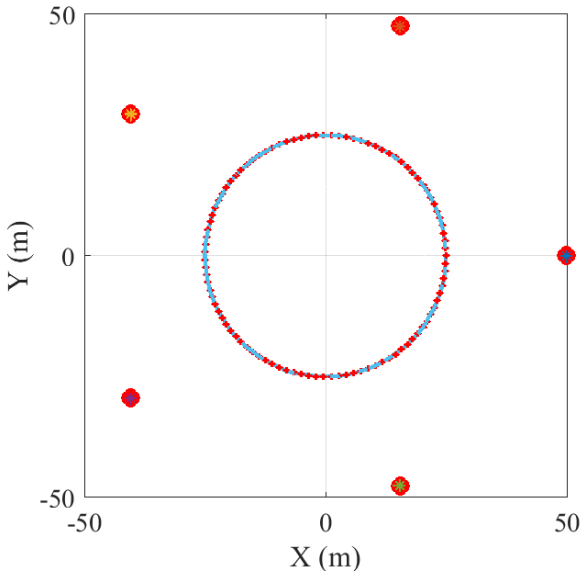


**Fig. 7 Second swarm geometry XY-plane with true locations (red) and estimated locations**

We can see in Fig. 8 that agents 1, 2, 3, and 4 have a slightly reduced standard deviation and error while agents 5 and 6 stay relatively the same. The Z-dimension of mobile agent 1 is also properly estimated with a median error close to 0. The reduced standard deviation can be attributed to increasing the total agent Z-dimension diversity. Mobile agent 1 and stationary agents 2 and 4 obviously benefit from this change as they are out of plane with the other agents while agent 3 benefits from the increased vertical angle by being the closest to agents 2 and 4.

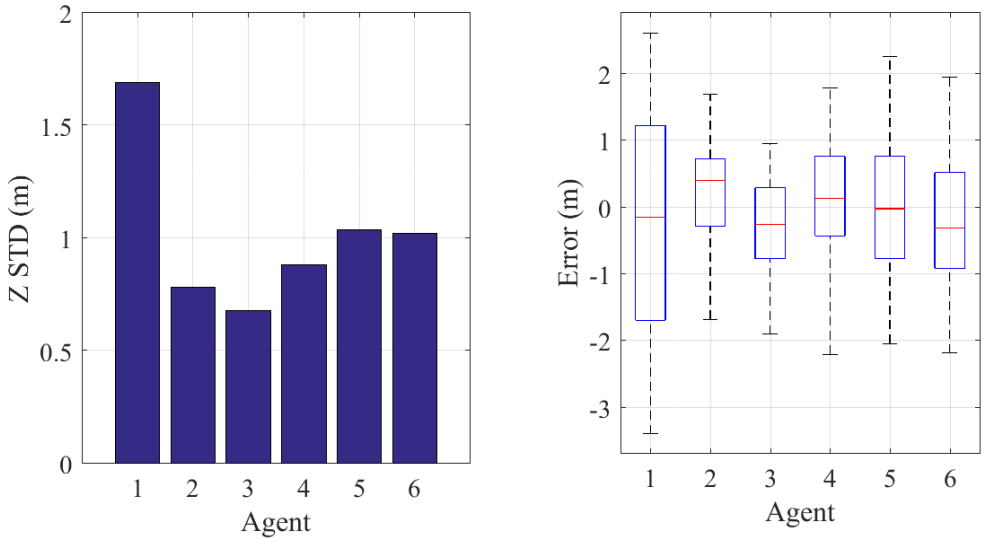


**Fig. 8 Standard deviation in Z (left) and position error (right) for the second swarm geometry in Figs. 6 and 7**

For Designs 3 and 4 we employ two concentric spheres, one inside the moving agent and one outside. The outside sphere is still fixed at 50 m with three agents equally spaced around its equator. For the center sphere we use 5- and 10-m radius spheres for Designs 3 and 4, respectively, with the two stationary agents equally spaced in the XY-plane and 2.5 m up in the Z-dimension. These configurations regain local symmetry with respect to the Z-offset of the stationary agents and move the stationary agents closer to the mobile node. Analysis of Design 2 demonstrated that moving two agents up in the Z-dimension while leaving them located on the outer sphere had only a small effect on reducing the error of the other stationary agents. Moving these agents onto a second inner sphere while also moving them up in the Z-dimension is expected to reduce DOP and therefore position error for the outer agents in comparison to Designs 1 and 2.

Figures 9 and 10 depict Design 3 in both the XZ- and XY-planes. It is clear in Fig. 9 that the deviation of the mobile as well as the three outer stationary agents has decreased. Figure 11 corroborates this as we can see the standard deviation and error for agents 1, 3, 5, and 6 have decreased while 2 and 4 have increased relative to our second design but decreased relative to the first. In addition, the median error for all agents is much closer to 0 when compared to the other two designs.

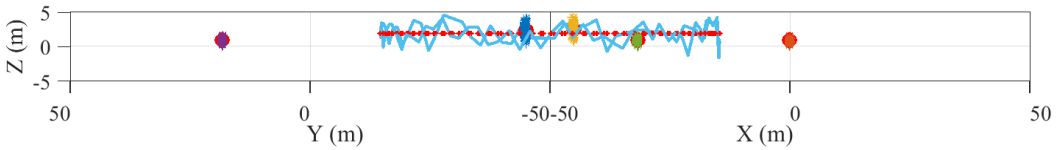


**Fig. 9 Third swarm geometry XZ-plane with a 45° perspective with true locations (red) and estimated locations**

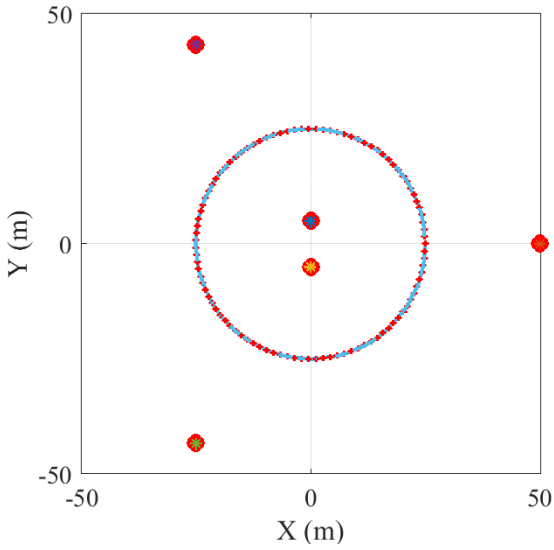


**Fig. 10 Third swarm geometry XY-plane with true locations (red) and estimated locations**

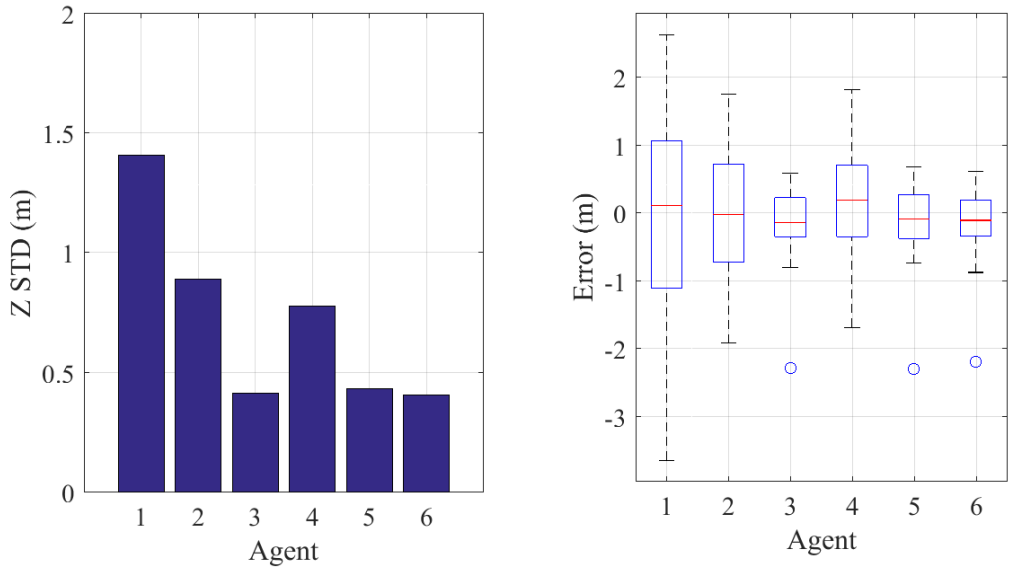


**Fig. 11 Standard deviation in Z (left) and position error (right) for the third swarm geometry in Figs. 9 and 10**

Design 4 has very similar performance to Design 3; however, by moving our inner stationary agents out by 5 m in each direction we trade a marginal increase in error on agents 2–6 for a small decrease in error for the mobile node by reducing the distance between it and the two inner stationary agents. This reduced distance increases the vertical angle between the mobile agent and inner agents 2 and 4. This is similar to the effect produced by agents 2 and 4 on agent 3 in Design 2. The geometry in Figs. 12 and 13 is our highest performing design (Fig. 14) and is used in the subsequent swarm experimental design.

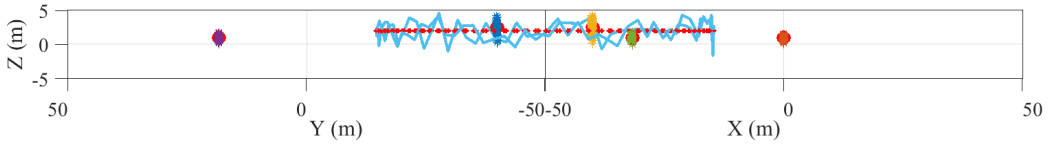


**Fig. 12 Fourth swarm geometry XZ-plane with a 45° perspective with true locations (red) and estimated locations**

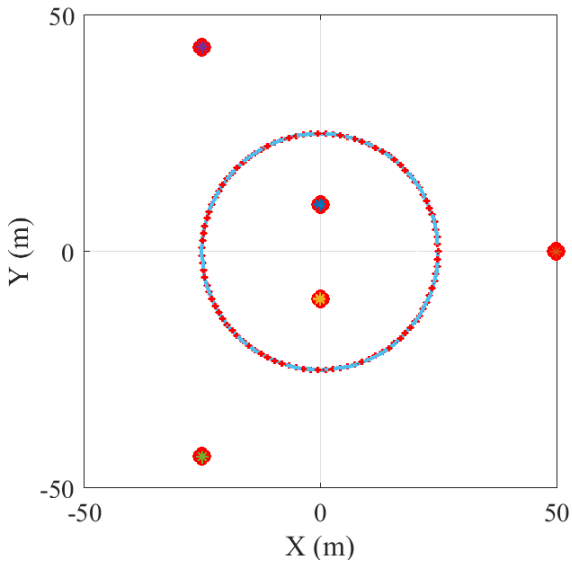


**Fig. 13 Fourth swarm geometry XY-plane with true locations (red) and estimated locations**

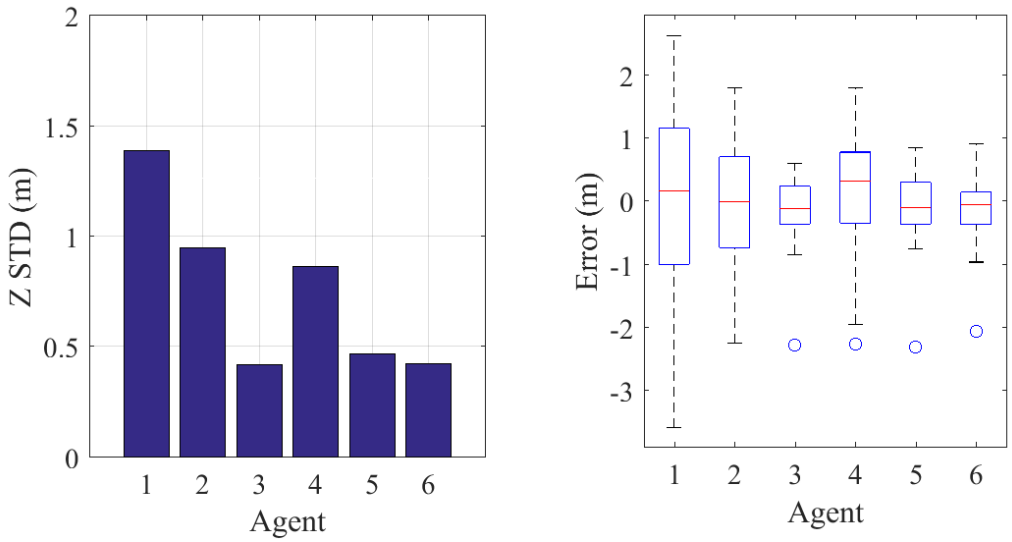


**Fig. 14 Standard deviation in Z (left) and position error (right) for the fourth swarm geometry in Figs. 12 and 13**

We analyze the DOP calculations of the mobile agent for the four constrained geometry designs by applying Eqs. 9 and 10 to our simulated position estimates. We see in Table 2 that Design 1 has the lowest ZDOP while simultaneously having the largest position RMSE. This can be explained by the limitations discussed previously with the MDS method. The remaining Designs 2–4 show standard behavior where DOP and RMSE decrease together.[1] Designs 3 and 4 have slightly

increased X and Y DOP because of the two center stationary agents are not sufficiently spread out to provide proper DOP in those dimensions to the mobile node. However, the reduced ZDOP more than makes up for the reduction in the other dimension.

**Table 2 DOP and RMSE values for four constrained geometry designs**

| Constrained geometry | XDOP | YDOP | ZDOP | RMSE |
|---|---|---|---|---|
| Design 1 | 0.64 | 0.64 | 19.4 | 0.46 |
| Design 2 | 0.67 | 0.69 | 27.0 | 0.38 |
| Design 3 | 0.73 | 0.73 | 22.8 | 0.29 |
| Design 4 | 0.72 | 0.72 | 22.3 | 0.29 |

# 4. Reliability Test in a Multipath Environment

## 4.1 Reliability Test Setup

Since dropped measurements due to low signal strength significantly impact the reliability of our relative swarm localization, it is important to choose an appropriate antenna for the ranging system and to verify that all of the devices perform similarly. First, a reliability experiment was conducted with three different antennas on our SwarmBee devices in a simple back and forth ranging test in a medium multipath environment at Aberdeen Proving Ground, Maryland, as seen in Fig. 15. We designate this space as "medium multipath" because of the presence of buildings, power lines, vehicles, and vegetation in the testing space. This test consisted of a static device mounted on a tripod at a height of 1 m at the start position in Fig. 15 and a moving unit that was walked down the shoulder of the road held at a height of 2 m for approximately 200 m. We tested the Blue Diamond 2.4-GHz patch antenna, a simple 1/4 wavelength (λ) whip antenna and a generic 2.4-GHz 1/2 λ antenna similar to those found on commercial Wi-Fi routers. The antennas under test were chosen for their different form factors. The antennas, shown in Fig. 16, and their antenna radiation patterns are included in Appendix A.


**Fig. 15 Outdoor reliability test walking procedure**

**Fig. 16 Antennas tested in the reliability experiment: 1/2 λ antenna (left), 1/4 λ whip antenna (middle), and the Blue Diamond patch (right)**

In addition, we repeated the same ranging test on all six SwarmBee devices using the 1/4 λ antenna to verify that all of the devices had similar performance. If any device exhibited substantially lower received signal strength or a high number of dropped ranges, it would indicate a hardware problem that should be rectified before a swarming experiment. The SwarmBee test device layout used in this and subsequent experiments is shown in Fig. 17.

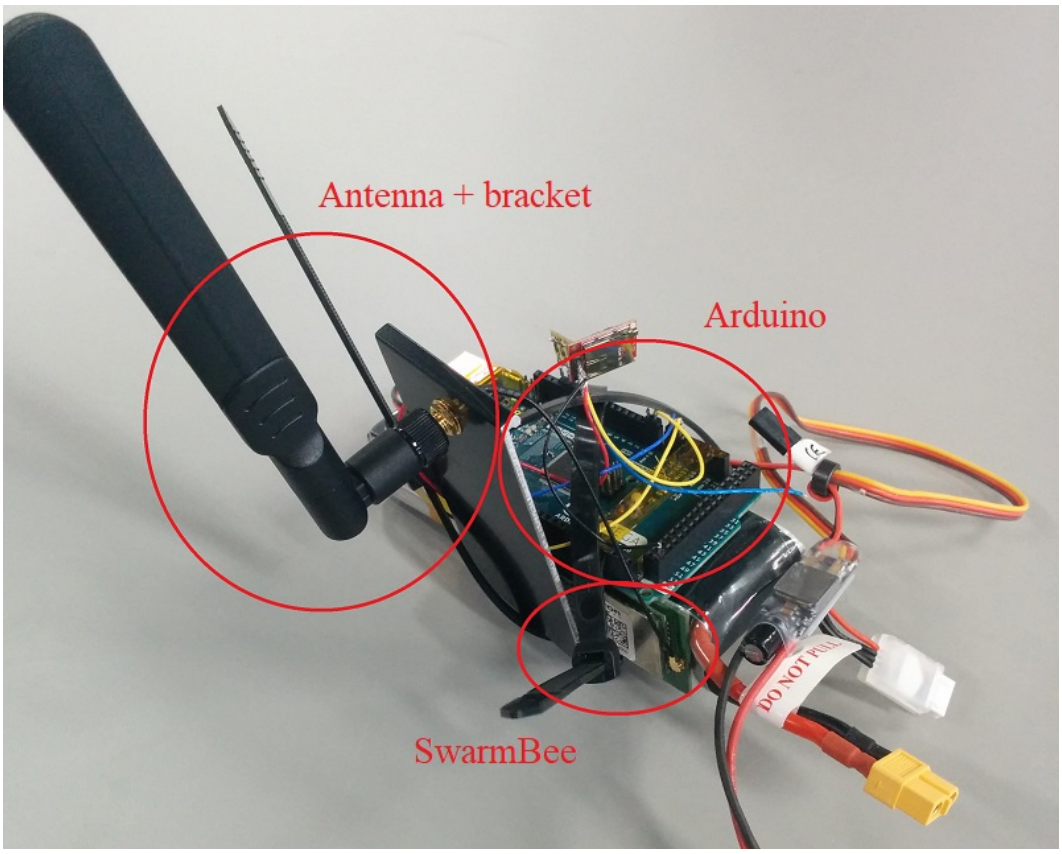


**Fig. 17 SwarmBee test device used in ranging experiments**

## 4.2 Reliability Test Results

In Table 3 we see reliability test results for the three antennas described in the previous section. For the Blue Diamond Patch we tested three different antenna orientations on the moving device with respect to the static device. We recorded the distance measurements, number of measurements, dropped measurements, and the device received signal strength indication (RSSI). For this preliminary test we have no reference distance measurements and therefore do not test range accuracy here. That analysis is conducted in the following section. We can see from the drop percentage alone that the dipole is the best performing antenna while the whip is the worst. The whip also has around 5 dB lower mean RSSI than the other antennas. Consequently, we conduct the unit consistency test using the 1/2 λ antenna. From

basic antenna knowledge and by examining the antenna radiation patterns in Appendix A, it was expected that the 1/2 λ antenna would perform similarly well to the 1/4 λ antenna in a horizontal configuration, and the Blue Diamond would perform the worst as it has significant loss in various horizontal positions, even though its peak gain is slightly higher. The difference between the theoretical and experimental results can be partially explained from the antenna mounting location as the 1/4 λ and Blue Diamond antennas have more strict mounting requirements. Additional plots showing dropped range measurements are shown in Appendix B.

**Table 3 Reliability test of different antennas**

| Antennas | Measurements | Drops | % Dropped | Mean RSSI |
|---|---|---|---|---|
| Blue diamond (front) | 1243 | 534 | 42.961 | –71.085 |
| Blue diamond (back) | 1206 | 638 | 52.902 | –71.722 |
| Blue diamond (edge) | 1202 | 489 | 40.682 | –71.285 |
| Monopole whip | 1135 | 909 | 80.088 | –76.549 |
| Large 2.4 GHz dipole | 1226 | 327 | 26.672 | –71.796 |

In Table 4 we can see the results of the same test procedure as before, this time with different SwarmBee modules. All six devices performed consistently well with device 1 and 6 performing slighting better and slightly worse, respectively. Since this test was conducted with medium vehicle traffic on the road, additional multipath likely played a part in the variation in percentage of dropped measurements as mean RSSI was consistent across all six units.

**Table 4 Reliability test of different SwarmBee devices**

| Antennas | Measurements | Drops | % Dropped | Mean RSSI |
|---|---|---|---|---|
| SwarmBee 1 | 1338 | 442 | 33.034 | –68.980 |
| SwarmBee 2 | 1348 | 501 | 37.166 | –70.240 |
| SwarmBee 3 | 1416 | 516 | 36.441 | –70.314 |
| SwarmBee 4 | 1373 | 477 | 34.741 | –71.049 |
| SwarmBee 5 | 1285 | 472 | 36.732 | –71.252 |
| SwarmBee 6 | 1286 | 581 | 45.179 | –70.879 |

# 5. Outdoor Long-Range Test

## 5.1 Range Test Setup

The maximum range for the SwarmBee device is specified by the manufacturer to be 500 m using a 1/4 λ antenna and our testing verified this maximum range. Additionally, we assessed the accuracy of the ranging measurement as a function of range. The antenna selection effort described previously was conducted in an environment that contained RF noise in the 2.4-GHz spectrum as well as a number

of objects that were likely to generate multipath effects. However, it is expected that for airborne applications multipath effects and RF interference will be more limited. Accordingly, a location was selected for the range performance test that was relatively free of RF interference and provided an unobstructed line of sight between ranging devices. This location consisted of an open field with a straight path 600 m long along the field edge. While an unobstructed line of sight was achieved along the entire length of the path, one heavily foliated tree was present adjacent to the path at a range of approximately 500 m. A spectrum analyzer was used prior to selection of this site to verify a low level of RF interference in the 2.4-GHz band. Additionally all devices associated with the test setup possessing Wi-Fi capabilities were configured to disable the Wi-Fi. The spectrum analyzer pictured later in Section 6.1 was used to collect a wideband measurement of the 2.4–2.5 GHz spectrum using peak-hold over 30 s at the time of the test to verify no devices were inadvertently transmitting in the 2.4-GHz band and interfering with the measurements. The results are shown in Fig. 18.

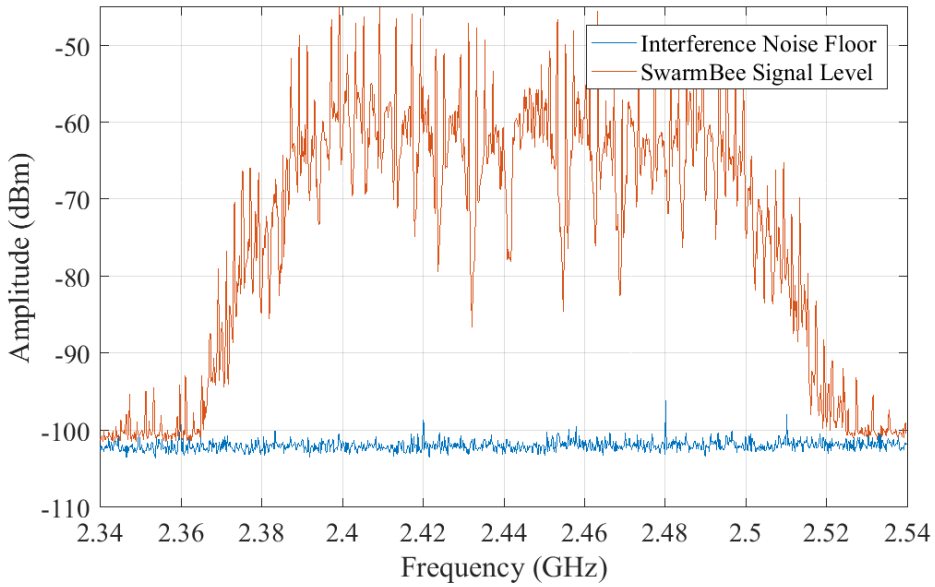


**Fig. 18 Power reading in dBm of 2.34–2.54 GHz spectrum at the test location. SwarmBee signal is measured 1 m from the spectrum analyzer.**

The antenna identified in the effort described previously as providing the best relative dropped range performance was used for the range test as well as for subsequent experiments. It is assumed that performance across other metrics will also be better than other antennas considered. Figure 19 depicts the test setup for the range test. A stationary device was attached to a laptop computer and used for data logging. A battery powered mobile unit like the one in Fig. 17 was manually carried out and back along the path.

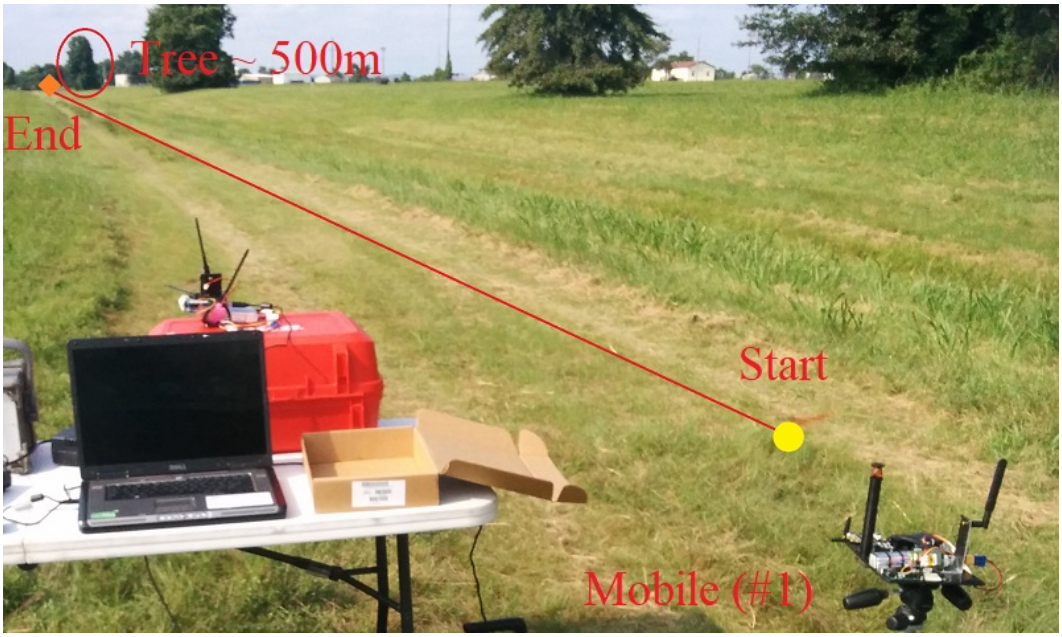


**Fig. 19 Long-range outdoor RF ranging test setup and walking procedure**

Effective evaluation of range performance and measurement accuracy requires a reference measurement of the position of the stationary and mobile TWR units. A Leica TS16 Robotic Total Station was used to take survey grade measurements of the position of each TWR unit. The TS16 combines the functionality of a theodolite and a laser rangefinder to measure the relative position of a reflective prism in three dimensions. The TS16 is capable of robotically tracking the prism and automatically measuring its position at rates up to 5 Hz. A 360° mini-prism was placed adjacent to the stationary TWR device and its position was recorded. The same mini-prism was then attached to the breadboard containing the mobile TWR device and its position was measured automatically by the TS16 for the duration of the test.

## 5.3 Range Test Results

We can see in Fig. 20 that the range test with the large 1/2 λ outperformed the manufacture specifications by achieving up to a 600-m range without significant errors in the ranging measurement. The large tree located at approximately 500 m appeared to generate a significant multipath effect, which when combined with the signal-to-noise ratio at that distance resulted in a large number of dropped measurements when the mobile TWR unit was near the tree. When the known distance using the total station survey equipment is superimposed on the RF ranges, the data agree well. Quantitatively, the distance measurements are very accurate, with only a 1.33-m RMSE over the whole test procedure with increasing error over

distance. The median error is strictly less than 0 for all distance, meaning the SwarmBee consistently underestimates the distance for a mobile agent. In the 49-m range, the error spread from the 25th to 75th percentiles is about 0.5 m, which roughly matches the 25th to 75th percentile spread of the simulated 0.1-$m^2$ variance. This will give a close correspondence between the simulated swarm localization error and the experimental error presented in the next section. This test also verified that the SwarmBee is quite susceptible to multipath and interference since only 5% of the range estimates were dropped in this benign environment, versus approximately 30% dropped measurements in the previous environment, even though the range at which the device was tested was much less.

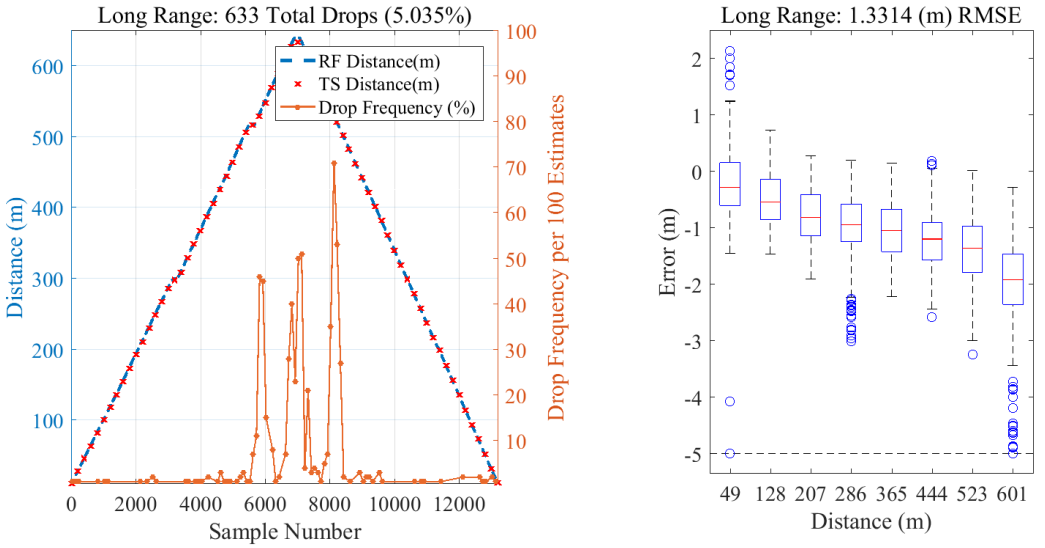


**Fig. 20 (left) SwarmBee distance estimate (blue) and dropped range frequency (orange) for mobile agent 1 superimposed on the true distance measurements from the total station (red x). (right) Distance error by distance in meters.**

# 6. Outdoor Swarm Localization Test

## 6.1 Swarm Test Setup

For the swarm relative localization test we install five stationary agents, called anchors in the subsequent figures, according to the highest performance constrained geometry simulation conducted previously. We used 1-m tripods and 2.5-m ladders to obtain the correct height in the Z-dimension. The locations of the anchor units were identified using a compass and a reference center point in the middle of the low multipath field on Spesutie Island located at the Aberdeen Proving Ground, Maryland. An aerial satellite view of the field can be seen in Fig. 21. Figures 22

and 23 show the locations of anchors 2 through 6, excluding 3. Anchor 3, the mobile agent 1, data logging station, and spectrum analyzer are shown in Fig. 24.

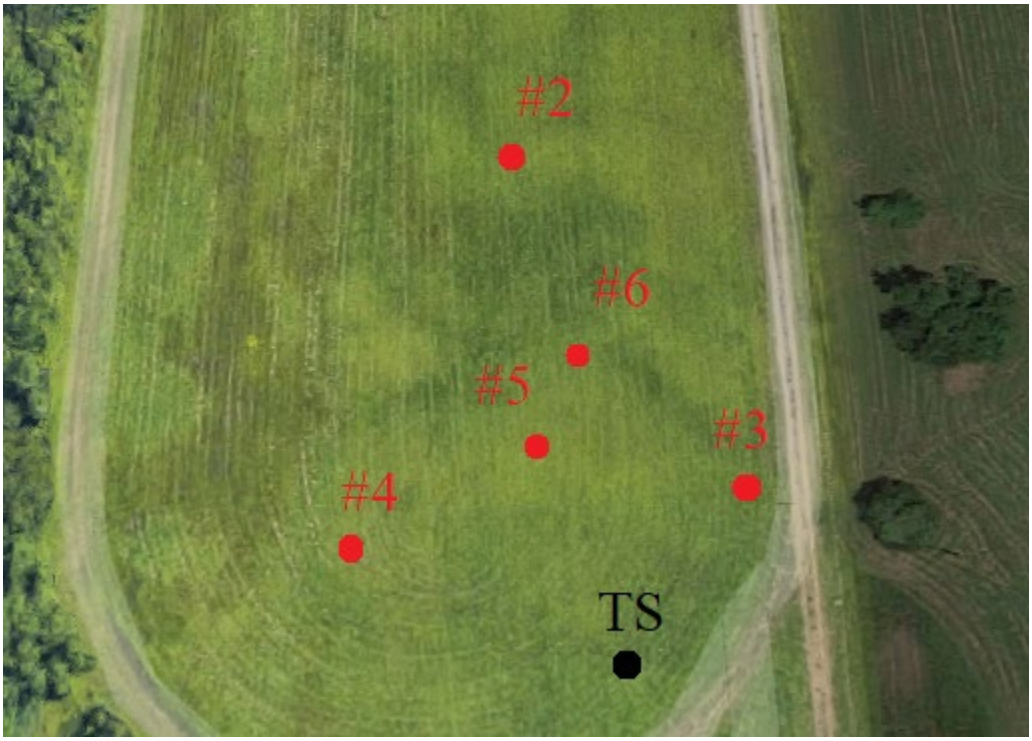


**Fig. 21 Low multipath field located on Spesutie Island. The TS16 total station survey equipment location is marked TS in black while the five stationary (anchor) agents are numbered and marked in red.**

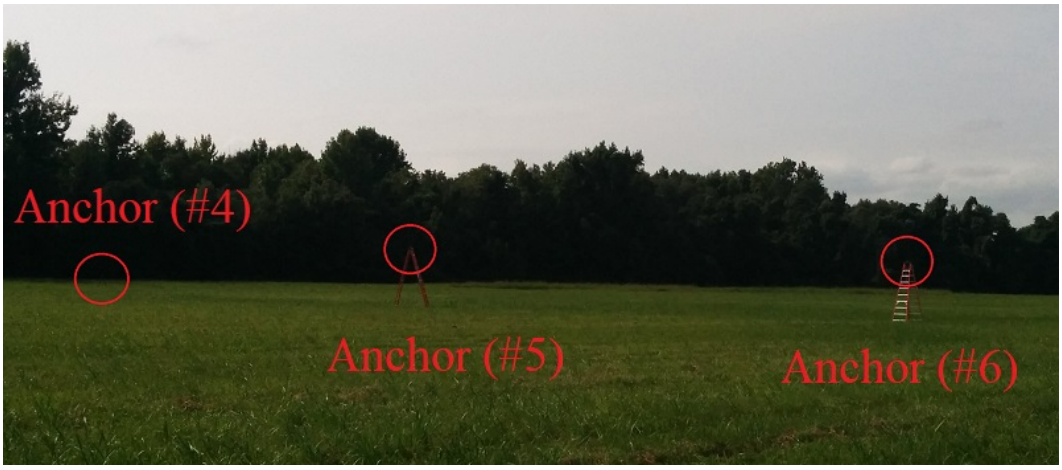


**Fig. 22 Swarm RF relative localization test range with three anchor agents 4, 5, and 6 visible**


**Fig. 23 Swarm RF relative localization test range with two anchor agents 6 and 2 visible**

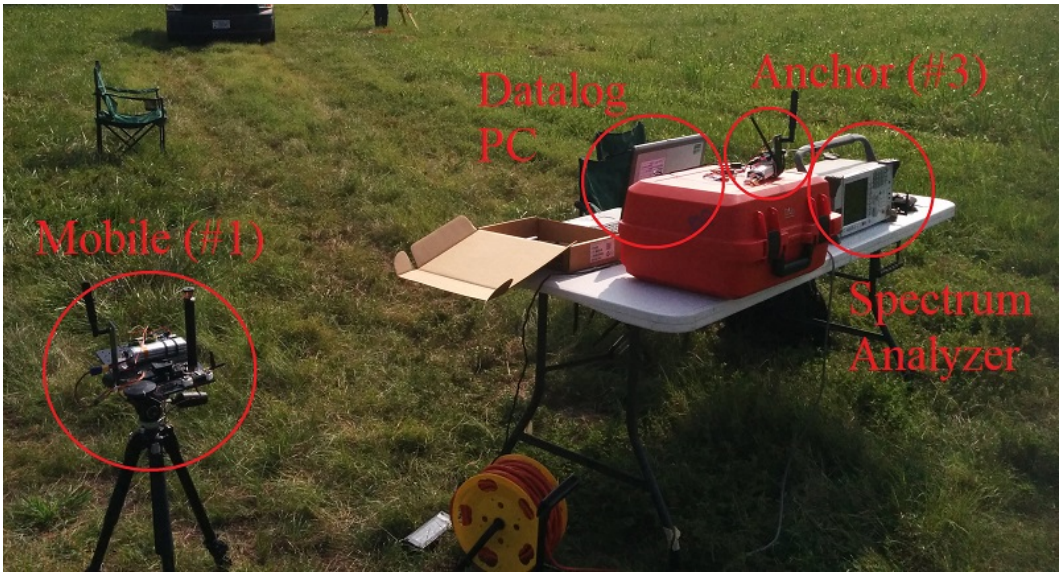


**Fig. 24 Swarm RF relative localization data collection station with the mobile agent, data logging PC, anchor agent 3, and the spectrum analyzer visible**

The TS16 total station pictured in Fig. 25 was used to collect position measurements of TWR devices. Positions of all the anchors were taken prior to testing and the mobile unit was tracked at 5 Hz while being carried at a walking pace in either a counterclockwise circle or a crisscross pattern between the anchors.


**Fig. 25 Swarm RF relative localization survey equipment (Leica TS16 Robotic Total Station) that records known positions in the (X,Y,Z) dimensions**

## 6.2 Swarm Test Results

The experimental results for the circle and crisscross walk tests can be seen in both the XZ- and XY-planes in Figs. 26 and 27 and Figs. 28 and 29, respectively. We can see that, as our simulations predicted, the XY position estimates are very precise while most of the variation is in the Z-dimension. Figures 30 and 31 show the Z-dimension standard deviation and position error for the circle walk and crisscross walk, respectively.

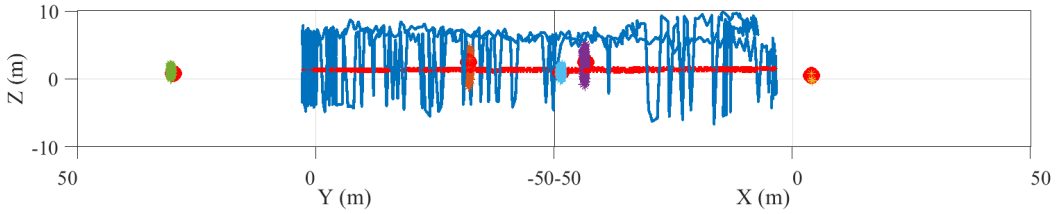


**Fig. 26 Experimental swarm geometry counter clockwise walk XZ-plane with a 45° perspective with true locations (red) and estimated locations**

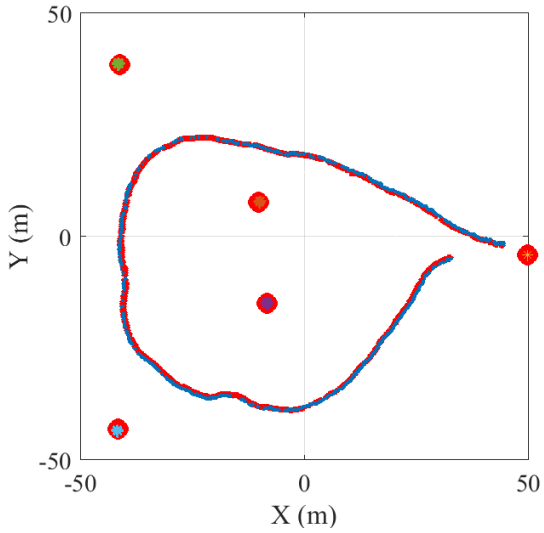


**Fig. 27 Experimental swarm geometry counter clockwise walk XY-plane with true locations (red) and estimated locations**

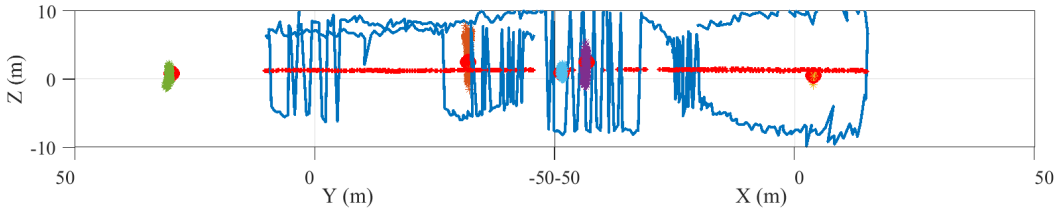


**Fig. 28 Experimental swarm geometry crisscross walk XZ-plane with a 45° perspective with true locations (red) and estimated locations**

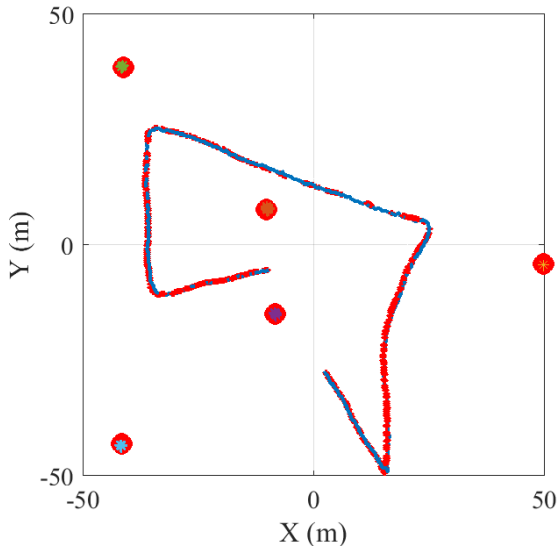


**Fig. 29 Experimental swarm geometry crisscross walk XY-plane with true locations (red) and estimated locations**

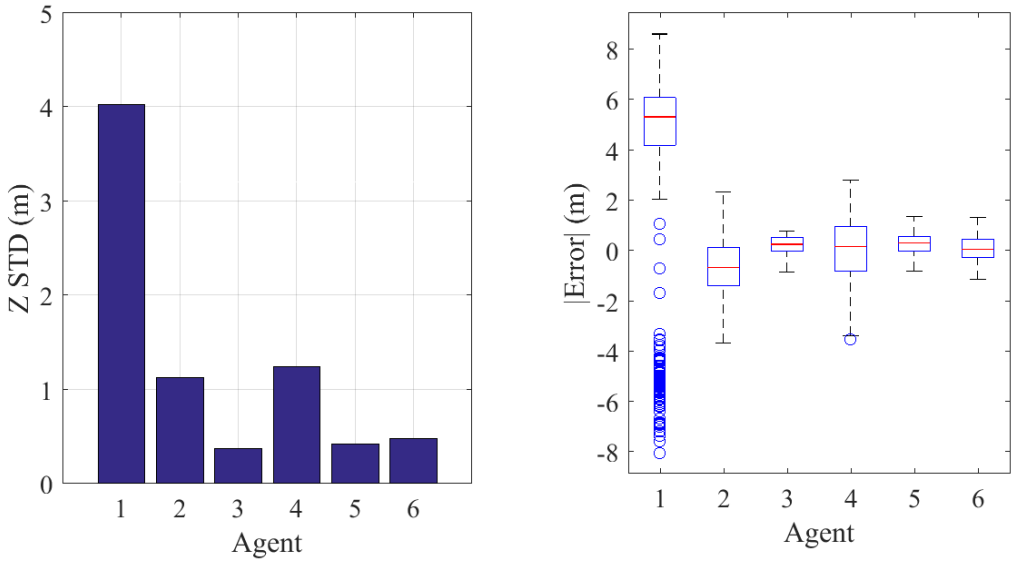


**Fig. 30 Standard deviation in Z (left) and position error (right) for the experimental swarm geometry counterclockwise walk in Figs. 26 and 27**

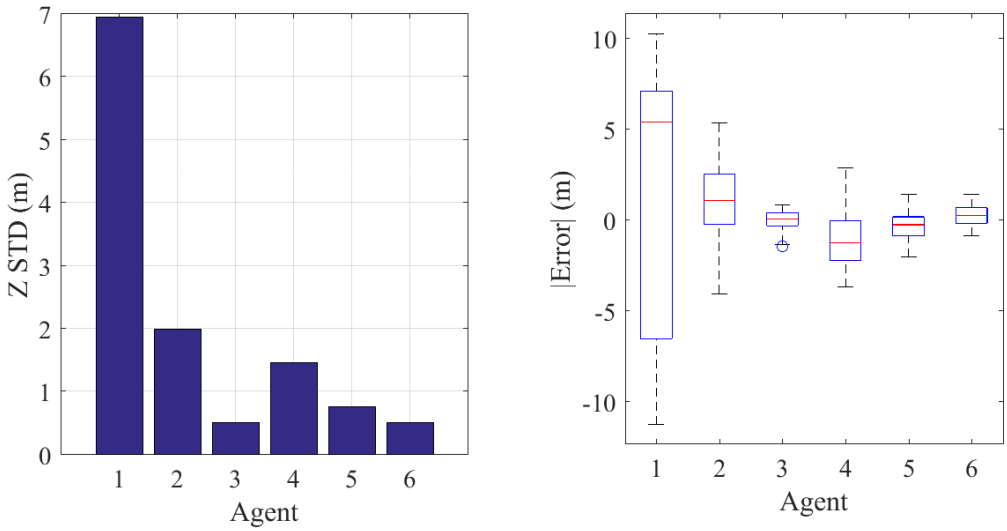


**Fig. 31 Standard deviation in Z (left) and position error (right) for the experimental swarm geometry crisscross walk in Figs. 28 and 29**

For the circle walk experiment, relative error and standard deviation between each agent also follows simulation. The mobile agent has the most error, agents 3, 5 and 6 have the least while agents 2 and 4 are in the middle. However, the mobile agent error is disproportionally large and greatly offset from 0 compared to what we see in simulation. In the circle walk test, the error for the middle stationary agents 2 and 4 are around 1 m, which is very close to the simulated positions using $\sigma^2 = 0.1$ noise with 0 mean on each distance estimate. Correspondingly, the error of the outer agents 3, 5 and 6 also agree with simulation at about 0.5-m mean error.

However, for the crisscross walk, position standard deviation for agents 2 and 4 increase to around 1.8 and 1.5 m, respectively, while agents 3, 5, and 6 stay relatively the same at 0.5 m. The mobile agent standard deviation is larger than the circle walk at around 7 m and the error median is also offset from 0 by 5.1 m. This is puzzling since measurement error should have stayed relatively the same as both tests were completed back to back in a benign environment. It is clear from these results that sudden change in mobile movement plays a large role in position estimation error when the DOP is poor.

To better understand the deviation of the experimental results from our simulations we analyze the statistics of the experimental data further. Table 5 shows the difference in mean between the SwarmBee stationary agents 2–6 estimated distances and the computed total station distances. It is clear that there is a slight bias that will have some effect on our computed distances since our original simulation did not account for error with a nonzero mean. To apply this to our simulation we create a matrix $\boldsymbol{M}_d \in \mathbb{R}^{6\times 6}$ and set the first row and first column

(mobile range means) to 0. The main diagonal is also 0 and the remaining elements follow those found in Table 5. We then add the means to the distance matrix $\boldsymbol{D}^{\odot 2}$ from Section 2. The variance of the stationary agent distances is also computed and is found to be 0.03. To account for this difference we set our Gaussian noise variance $\sigma^2$ in our simulation equal to 0.03. An example of the noise and mean offset seen on the distance measurements per sample number are shown in Fig. 32 for stationary agents 2 to 3. Additionally, the distance error for the same samples is shown in Fig. 33. We can clearly see from this example that the stationary node distance mean is also slightly time variant; however, we do not account for this behavior in the simulation.

**Table 5 Difference in mean between SwarmBee distances and total station (meters)**

| Devices | SwarmBee 2 | SwarmBee 3 | SwarmBee 4 | SwarmBee 5 | SwarmBee 6 |
|---|---|---|---|---|---|
| SwarmBee 2 | … | –0.32 | –0.17 | 0.12 | 0.41 |
| SwarmBee 3 | –0.33 | … | 0.13 | 0.59 | 0.36 |
| SwarmBee 4 | –0.18 | 0.12 | … | 0.17 | 0.24 |
| SwarmBee 5 | 0.11 | 0.61 | 0.17 | … | 0.51 |
| SwarmBee 6 | 0.41 | 0.35 | 0.24 | 0.51 | … |

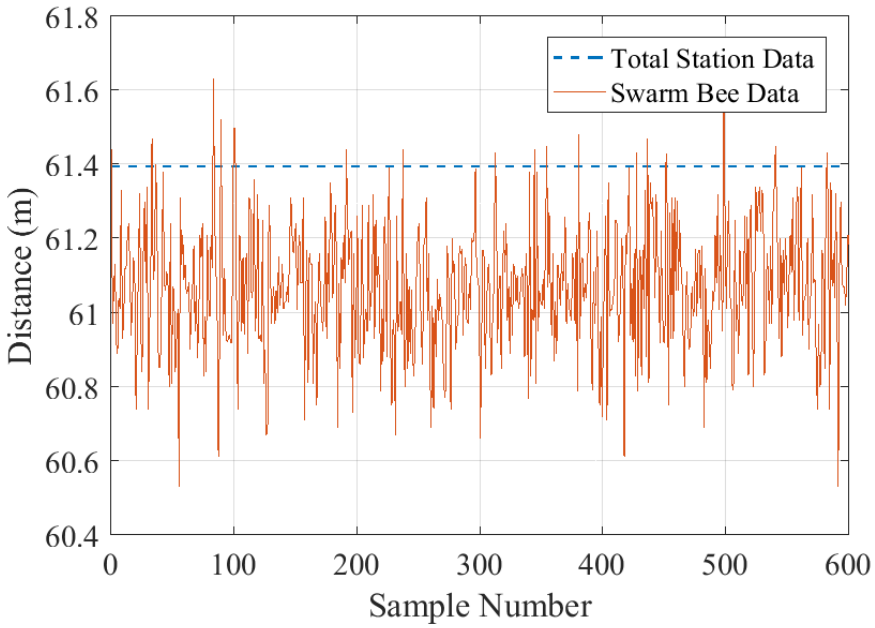


**Fig. 32 Computed distance vs. sample number from stationary agent 2 to stationary agent 3**

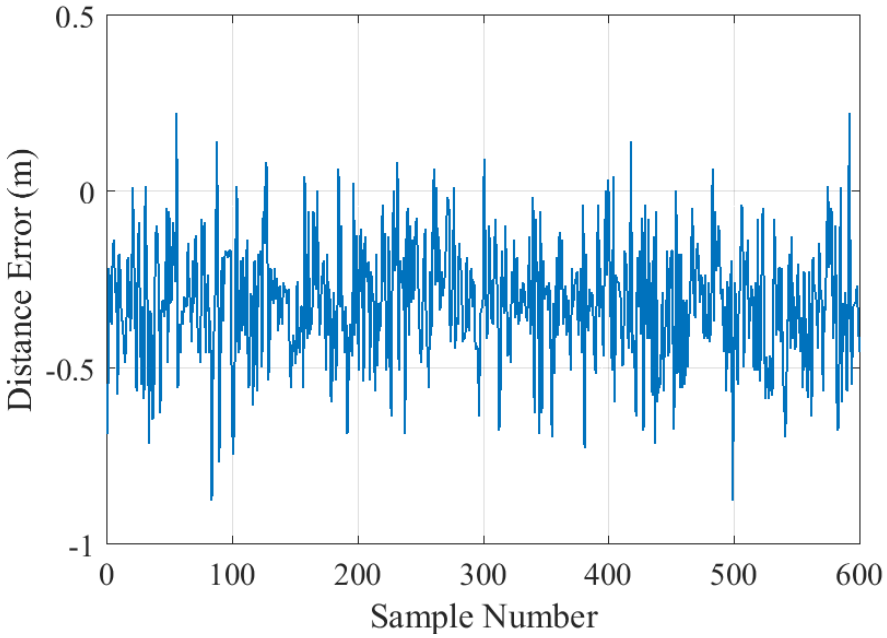


**Fig. 33 Computed distance error for stationary agent 2 to stationary agent 3**

The mobile agent distance statistics are also analyzed and found to have a value either above or below the true trajectory throughout the circle walk test. Figure 34 shows a subset of samples taken from the circle walk test farthest from stationary agent 3, while Fig. 35 shows the distance error for those samples. The maximum overshoot and undershoot distance is around 1 m while the average overshot and undershot distance estimate is 0.85 m over the whole circle walk. The crisscross walk has slightly different statistics with its mobile agent distance estimate offset changing more rapidly. In order to account for this behavior in our simulation we apply a uniform random integer value on the interval [0,1] to the first row and first column of $\boldsymbol{D}^{\odot 2}$ for all simulated distance measurements excluding the element $d_{1,1}$, which is set to 0. The random variable is further scaled by 0.85 to match our experimental data. This distance offset added to each measurement between the mobile and stationary agents over time is drawn from the same distribution.

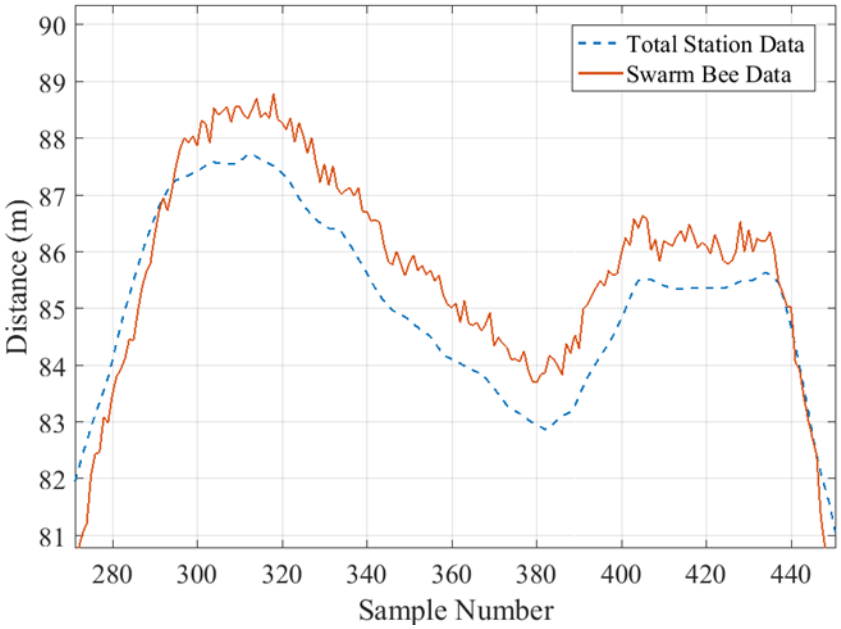


**Fig. 34 SwarmBee distance estimate and total station computed distance from agent 1 (mobile) to stationary agent 5**

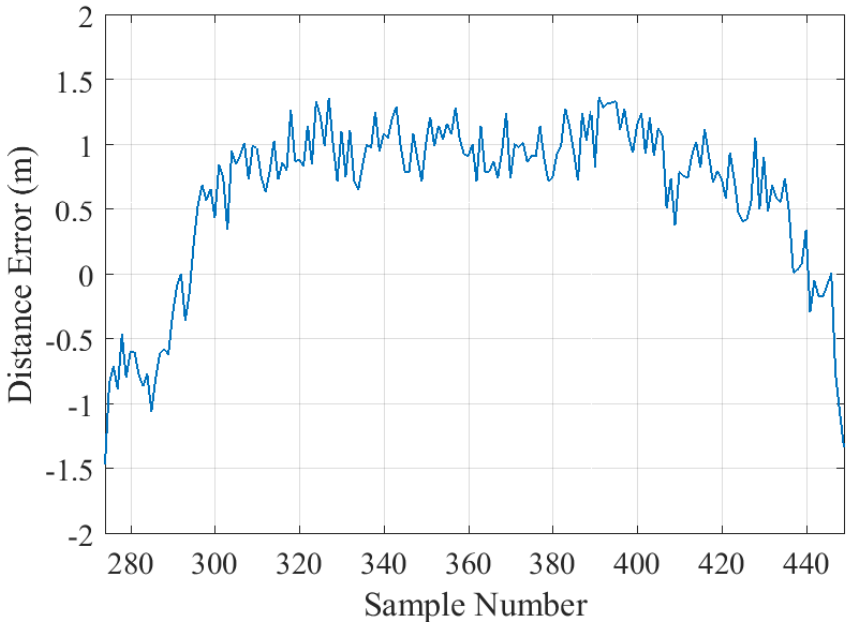


**Fig. 35 SwarmBee distance error of agent 1 (mobile) to stationary agent 5**

The results of the updated simulation with these noise modifications applied can be seen in Figs. 36–38. For the circle walk test the position estimates, standard deviation and error now more closely follow our simulation data in Figs. 26, 27, and 29. A small distance bias of about a meter on the mobile agent can have a very

large impact on the Z-dimension position estimate using the MDS method because of the significant ZDOP of the swarm. Although the stationary agents also experience distance bias as seen in Table 5, they do not contribute significantly to any position error as the Kabsch algorithm in Eqs. 5–10 aligns the position estimates of the whole swarm to the stationary nodes, which minimizes their position RMSE.

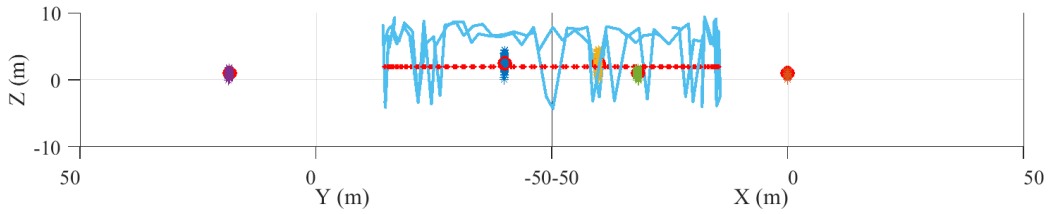


**Fig. 36 Fourth swarm geometry XZ-plane with a 45° perspective with true locations (red) and estimated locations using modified measurement noise**

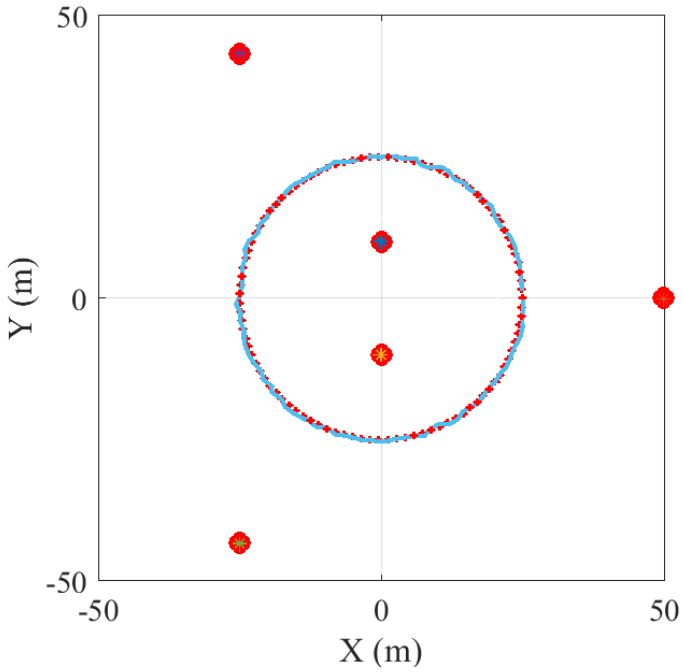


**Fig. 37 Fourth swarm geometry XY-plane with true locations (red) and estimated locations using modified measurement noise**

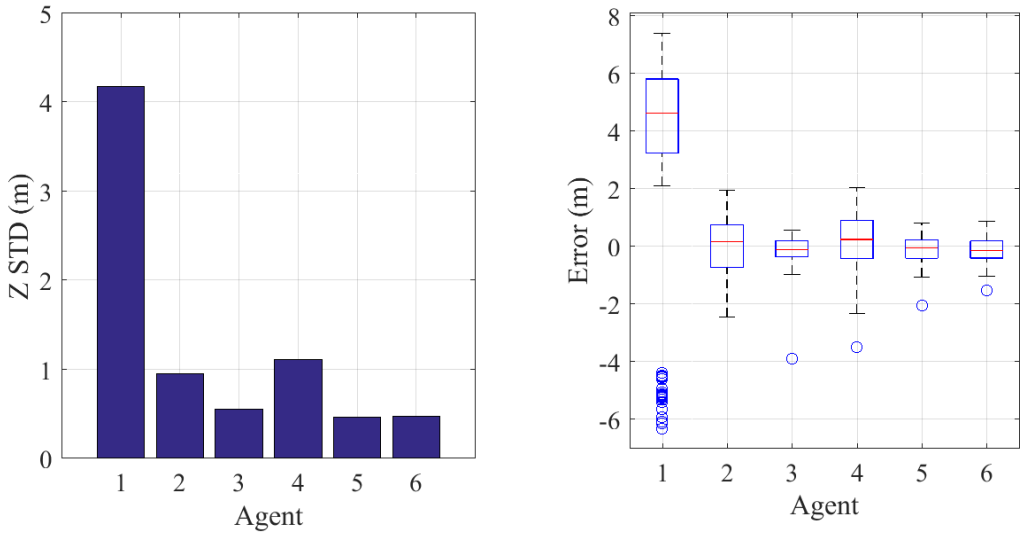


**Fig. 38 Standard deviation in Z (left) and position error (right) for the fourth swarm geometry with modified measurement noise in Figs. 36 and 37**

Additionally, when analyzing the data logging procedure of the SwarmBee agents from the previous work, we found that the SwarmBees are only capable of ranging to a single device at a time, therefore causing the elements of the distance matrix $\boldsymbol{D}^{\odot 2}$ to be be slightly time variant. We did not account for this in our updated simulation but it is assumed to be a problem as mobile agent speed or number of swarm agents increases, which would reduce the distance update speed.

## 7. Conclusion

Building on previous work on swarm relative localization[1,13] we have designed a constrained geometry and evaluated it using simulated position error and computed its DOP. We find that suboptimum constrained geometries exhibit exceptionally high ZDOP thanks to the strict constraints on the number of agents and agent position in Euclidean space. Correspondingly, position error varies for different agents in the swarm depending on their location within the swarm geometry. The geometries still exhibit excellent XDOP and YDOP, which are reflected in the high position accuracy in those dimensions throughout the experiment.[1]

We also experimentally evaluated the SwarmBee devices in different environments and concluded that dropped ranges are highly correlated to multipath effects. The SwarmBee devices are also accurate within their manufacturer specified range of 500 m. However, even though the position accuracy is within 2 m of the total station reference locations in a two-way walk test, there is a bias present that increases with distance. When using the SwarmBee TWR device measurements as experimental data in our relative localization algorithms we find that the position error does not

accurately follow the original simulation containing a mobile node with simple Gaussian noise added directly to the range measurements, due to the bias from the SwarmBee devices. This difference was accounted for in simulation by analyzing the experimental data statistics and modifying our simulation accordingly. Additional effects like time-varying mean and time variation in our distance estimates caused by the SwarmBee ranging protocol[13] are not accounted for in the research but are left for future work on the subject. The results of this experiment lead to exciting future research questions, including the following:

- Can the relative localization methods used in this research be modified to reduce or remove the effects of the agent distance bias on position estimates?
- Can time-varying effects of the estimated agent distance mean and distance matrix be properly characterized in simulation?
- What are the effects on position error of increasing the number of SwarmBee agents, the mobile agent velocity, and the range measurement update rate?

Although very promising preliminary results have been obtained in this study, more research and development needs to be conducted to improve the real performance of relative swarm localization with constrained geometries.

## 8. References


1. Don ML. Dilution of precision as a geometry metric for swarm relative localization. Aberdeen Proving Ground (MD): Army Research Laboratory (US); 2017 Nov. Report No.: ARL-TR-8200.

2. Kurazume R, Nagata S, Hirose S. Cooperative positioning with multiple robots. In: Robotics and Automation. Proceedings of the 1994 IEEE International Conference on Robotics and Automation; 1994 May 8–13; San Diego, CA.

3. Young-Bae K, Vaidya NH. Location-aided routing (LAR) in mobile ad hoc networks. Wireless Networks 6.4. 2000:307–321.

4. Parker R, Valaee S. Vehicular node localization using received-signal-strength indicator. IEEE Transactions on Vehicular Technology. 2007;56(6):3371–3380.

5. Ryan A, Zennaro M, Howell A, Sengupta R, Hedrick JK. An overview of emerging results in cooperative UAV control. Proceeds of the 2004 43rd Conference on Decision and Control; 2004 Dec 14–17; Nassau, Bahamas.

6. Fresconi F, Fermen-Coker M. Delivery of modular lethality via a parent-child concept. Proceedings of the AIAA Atmospheric Flight Mechanics Conference; 2015 June 22–26; Dallas, TX. AIAA 2015-2708.

7. Langley RB. Dilution of precision. GPS World 10.5. 1999:52–59.

8. Misra P, Burke BP, Pratt M. GPS performance in navigation. Proceedings of the IEEE. 1999;87(1):65–85.

9. Iliev N, Paprotny I. Review and comparison of spatial localization methods for low-power wireless sensor networks. IEEE Sensors Journal. 2015;15(10):5971–5987.

10. Wickelmaier F. An introduction to MDS. Aalborg (Denmark): Sound Quality Research Unit, Aalborg University; 2003 May 4. http://www.mathpsy.uni-tuebingen.de/wickelmaier/pubs/Wickelmaier2003SQRU.pdf.

11. Kabsch W. A solution for the best rotation to relate two sets of vectors. Acta Crystallographica Section A. 1976;32:922–923.

12. Lockspeiser JR, Don ML, Hamaoui M. Radio frequency ranging for swarm relative localization. Aberdeen Proving Ground (MD): Army Research Laboratory (US); 2017 Oct. Report No.: ARL-TR-8194

13. Björck Å. Numerical methods for least squares problems. Philadelphia (PA): Society for Industrial and Applied Mathematics; 1996.

# Appendix A. Antenna Radiation Patterns

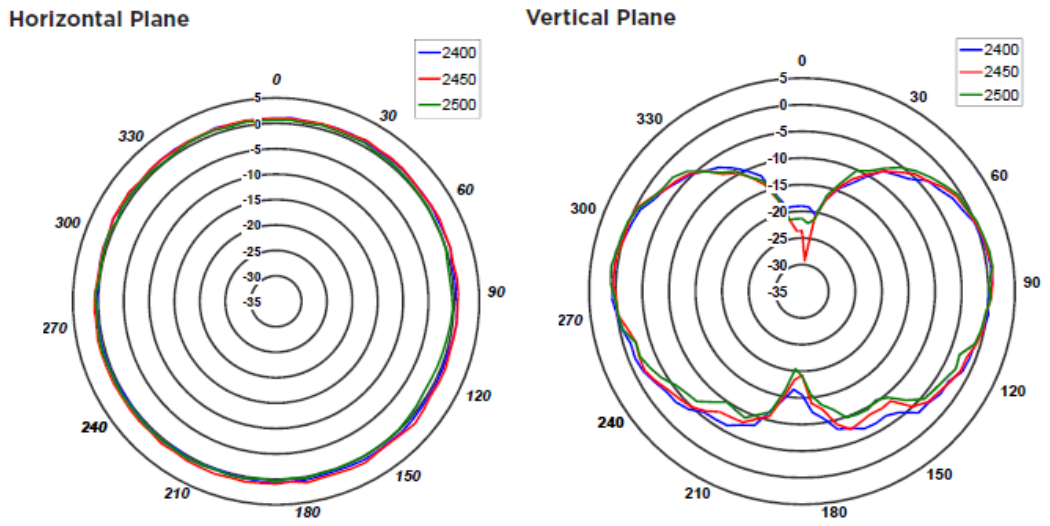


**Fig. A-1 Horizontal (left) and vertical (right) radiation pattern for the 1/2 λ antenna in the 2.4-GHz band. The peak horizontal gain at 2.4 GHz is 2 dBi.**[1]

[1] PulseLarsen Antennas. Wireless external dual band antenna for 2.4 GHz and 5.0 GHz applications. Datasheet. San Diego (CA): Pulse Electronics; c2013 [accessed 2019 Nov 27]. http://productfinder.pulseeng.com/products/datasheets/L148.pdf.

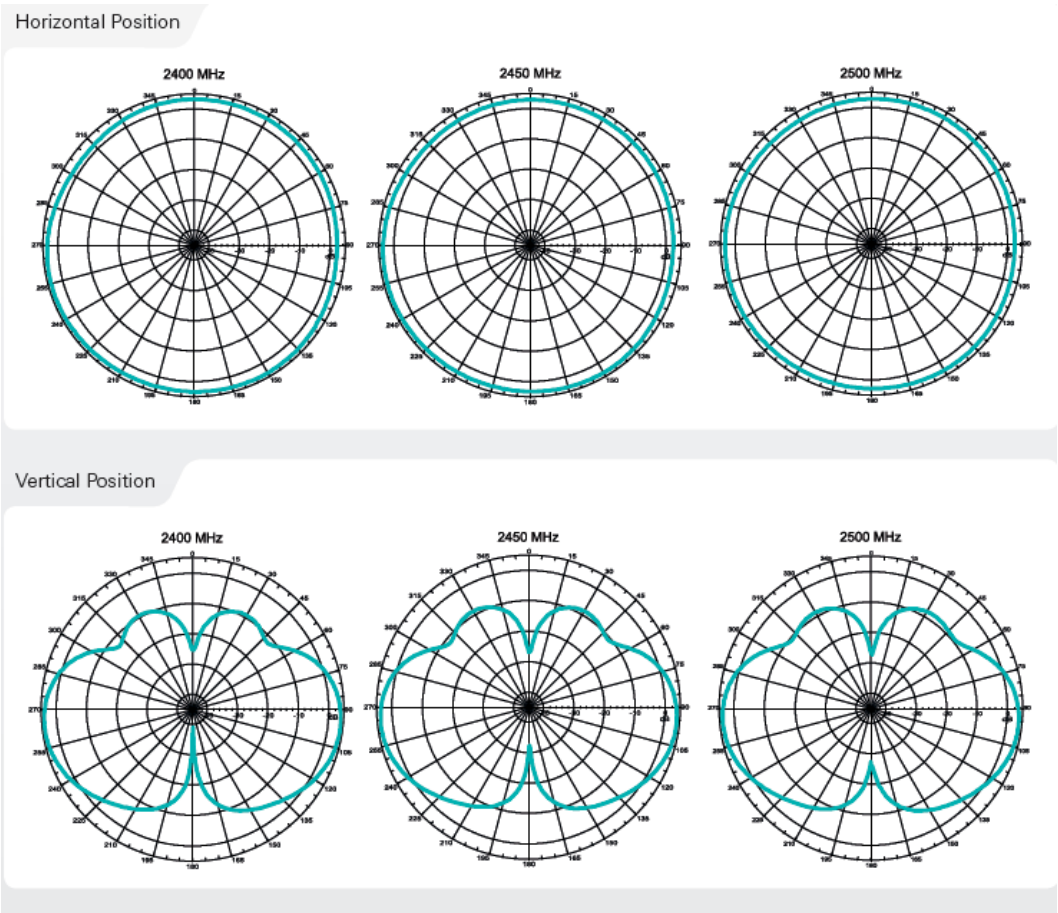


**Fig. A-2 Horizontal (top) and vertical (bottom) radiation pattern for the 1/4 λ whip antenna in the 2.4-GHz band. The peak horizontal gain at 2.4 GHz is 2 dBi.**[2]

[2] PulseLarsen Antennas. 2.4–2.5 monopole swivel stick antenna. Datasheet. San Diego (CA): Pulse Electronics; n.d. [accessed 2019 Nov 27]. http://productfinder.pulseeng.com/products/datasheets/W1030.pdf.

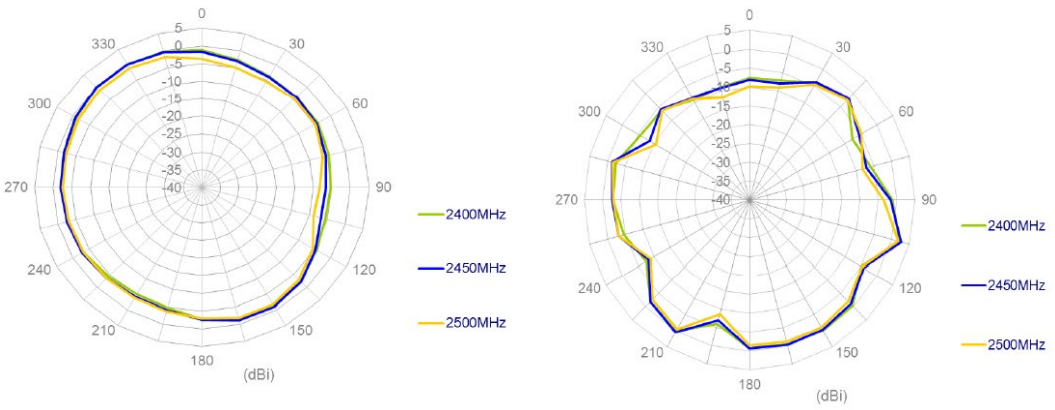


**Fig. A-3 Horizontal (left) and vertical (right) radiation pattern for the Blue Diamond patch antenna in the 2.4-GHz band. The peak horizontal gain at 2.4 GHz is 3 dBi.[3]**

[3] TAOGLAS. FXP73 Blue diamond 2.4 GHz band antenna. San Diego (CA): TAOGLAS; c2019 [accessed 2019 Nov 27]. https://www.taoglas.com/product/blue-diamond-fxp73-2-4ghz-flex-pcb-antenna-mmcxmra/.

# Appendix B. Dropped Range Measurements

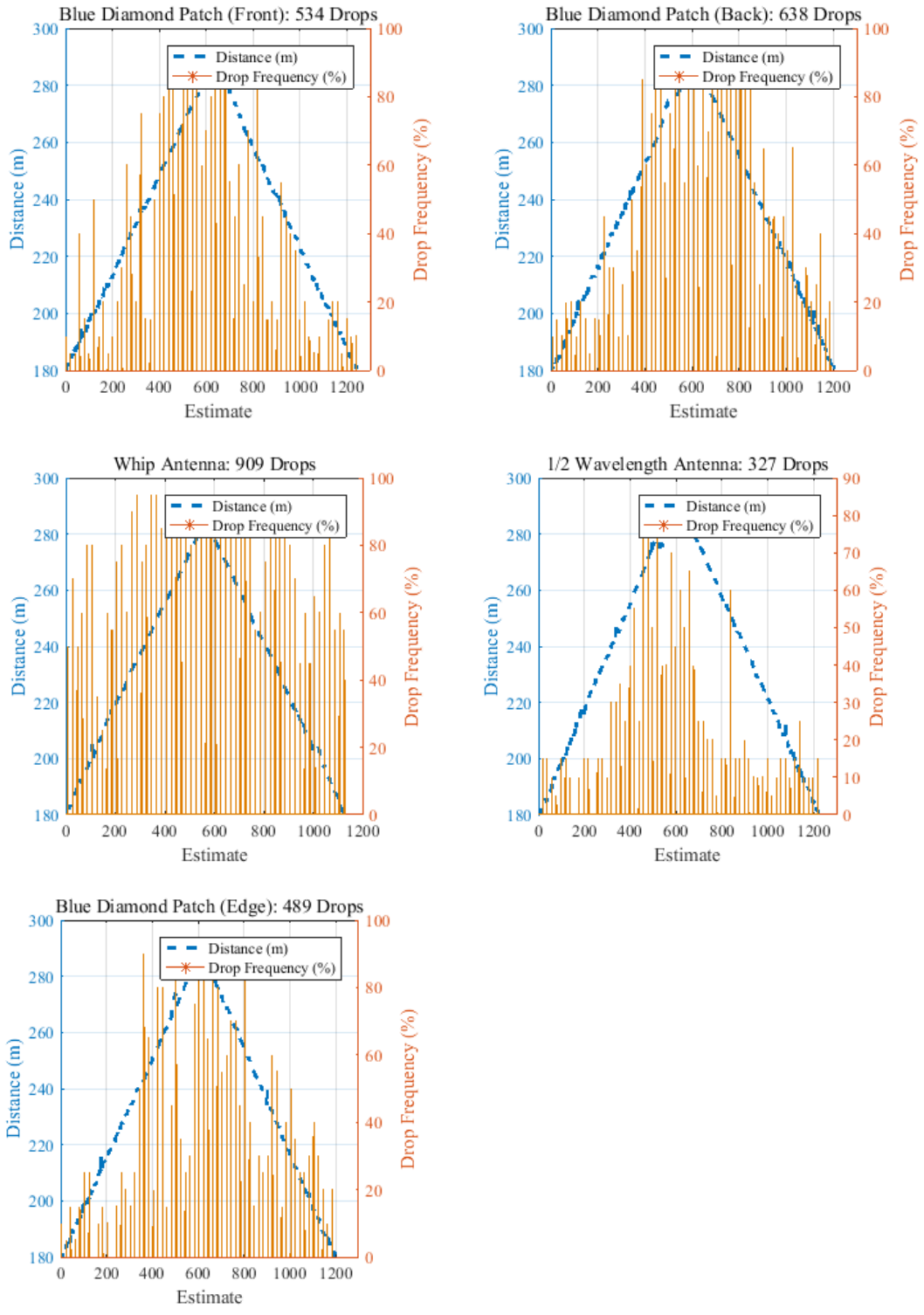


**Fig. B-1 Dropped ranges and distance estimate vs. range estimate for five reliability test cases**

## List of Symbols, Abbreviations, and Acronyms

| | |
|---|---|
| 2-D | two-dimensional |
| DOP | dilution of precision |
| GPS | global positioning system |
| MDS | multidimensional scaling |
| PDOP | position DOP |
| RF | radio frequency |
| RMSE | root mean square error |
| RSSI | received signal strength indication |
| TOF | time-of-flight |
| TWR | two-way ranging |
| XDOP | X-dimension DOP |
| YDOP | Y-dimension DOP |
| ZDOP | Z-dimension DOP |
| λ | wavelength |

| | |
|---|---|
| 1 (PDF) | DEFENSE TECHNICAL INFORMATION CTR DTIC OCA |
| 1 (PDF) | CCDC ARL FCDD RLD CL TECH LIB |
| 3 (PDF) | CCDC ARL FCDD RLW LF M GRABNER M DON D EVERSON |